Journal of Engineering and Applied Sciences 14 (Special Issue 2): 5420-5428, 2019
ISSN: 1816-949X

Comparative Study: Co_2 Sensing of Palladium Nanoparticles Grown on Normal and Gradient Porous Silicon

Alwan M. Alwan, Muslim F. Jawad and Duaa A. Hashim
Department of Applied Science, University of Technology, Baghdad, Iraq
Phone No./07702687313 and Email:/ahdu.8589@gmail.com

Abstract: In this research, normal Porous Silicon PSi layers and Gradient-Porous Silicon GPSi layer modified with Pd nanoparticles was used to produce an effective gas sensor. PSi and GPSi were fabricated using Laser-Assisted Etching process (LAE) on n-type silicon substrate. In PSi layer a laser diode of 630 nm wavelength and illumination intensity of about 25 mW/cm^2 at a fixed etching current density of 25 mA/cm^2 was employed. A step-gradient current density ranging from 25 to 5 mA/cm^2 at a fixed laser illumination intensity 25 mW/cm^2 was used to prepare GPSi. The surface morphology of bare PSi and GPSi and modified with Pd NPs were examined using Scanning Electron Microscopy (SEM), X-ray Diffraction (XRD), FTIR spectroscopy and EDS analysis. Electrical properties (J-V) of bare PSi, GPSi and modified with Pd nanoparticles were measured in vacuum and with CO_2 pressures of (0.5 and 1mbar) at room temperature. The result showed that the nanoparticles sized and substrate morphology strongly affected the sensor performance. It was found that the sensitivity of the sensor with modified GPSi is twice than the sensitivity of PSi due to the high density of dangling bonds at the interface of the silicon matrix.

Key words: Gradient Porous Silicon (G-PSi), Normal Porous Silicon (N-PSi), laser assisted etching, sensitivity, dangling bonds, Illumination, morphology

INTRODUCTION

PSi is a Nano-crystalline Si with voids there in is commonly fabricated by the electrochemical etching of the crystalline silicon wafer in ethanol or aqueous Hydrofluoric acid (HF) based electrolytes (Ogata *et al*., 2007). The high specific surface area and high chemical activity of PSi make them to be an interesting candidate for different applications, especially for gas sensing for environmental monitoring and protection. Indeed, these properties permit PSi to effectively react with gases. The adsorption of gas molecules at the nanowire surface entails a change in the conductivity which serves as the basis for molecular gas sensing (Ahmed *et al*., 2015). GPSi is a new form of partial type of porous silicon in which the pore cross-section and structure varies with depth (Starkov and Gavrilin, 2007). It has an excellent characteristic, especially in the field of solar cell Antireflection Coating (ARC) technology (Striemer and Fauchet, 2002), gas sensors (Hwang *et al*., 2011) and rugate filter applications (Fabricius, 1992). The preparation of metallic nanostructures gas sensors based on the surface features of porous layer is a very important choice to fabricate an efficient, low-cost and simple gas sensors. The surface properties like pores over shape, density of dangling bond (growth nucleation sites) of PSi and GPSi plays an important role in the growth of the deposited metal nano layer and hence, the sensor's performance of modified hetro structure gas sensor involving PSi and GPSi layer (Alwan *et al*., 2018; Alwan, 2014a, b). The effect of incorporating gold nanoparticles within the normal porous structures was studied by Alwan *et al*. (2017), they found that the sensory activities depend on the morphological properties of the deposited layer.

In this study, Pd/ PSi and Pd/ GPSi hetro structure gas sensor were fabricated as a gas sensor. Electrical properties of PSi layer and GPSi layer, barrier height, ideality factor and D_s state density (dangling bonds) were extracted using I-V characteristics before incorporating nanoparticles for two types of PSi layer. The Pd/ PSi and Pd/ GPSi hetro structure gas sensor performances were investigated based on the properties of the deposited metal nano layer.

MATERIALS AND METHODS

Figure 1 shows typical (LAE) process setups were used to prepare two types of normal Porous Silicon (PSi) and Gradient Porosity Porous Silicon (GPSi).

Preparation of normal Porous Silicon (PSi): Normal-layer PSi structure was prepared on (n-type) silicon wafer by a

Corresponding Author: Alwan M. Alwan, Department of Applied Science, University of Technology, Baghdad, Iraq
Phone No./07702687313 and Email:/ahdu.8589@gmail.com

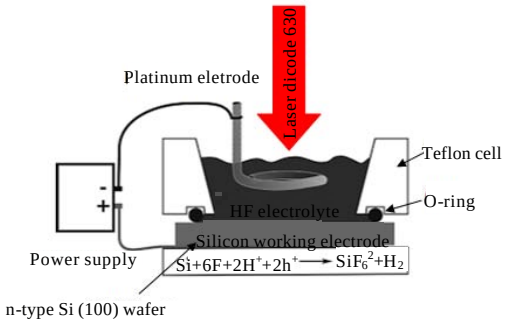

Fig. 1: Preparation setup of porous silicon layer

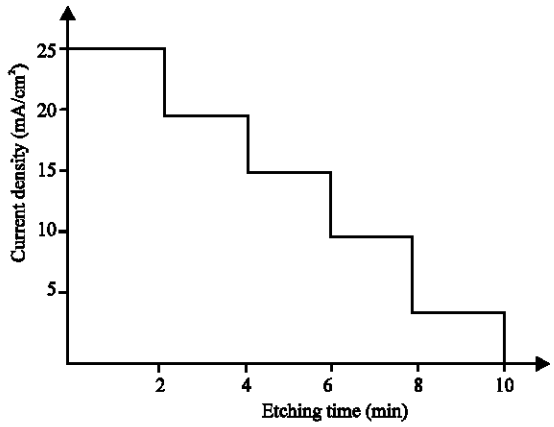

Fig. 2: Step gradient variation of current density in etching time

Laser-Assisted Etching (LAE) process. In this technique, PSi was dipped into a mixture of HF: Ethanol (1:1) with a concentration of (24%). Ethanol was added to the (HF) solution in order to improve the wet ability of the acid and to allow for the F^- ion's diffusion into pores (Alwan *et al*., 2017). In PSi layer a laser diode of 630 nm wavelength and illumination intensity of about 25 mW/cm^2 at a fixed etching current density of 25 mA/cm^2 was employed.

Preparation of Gradient Porous Silicon (GPSi): GPSi was prepared to step-gradient current density ranging from (25-5mA/cm^2) at a fixed laser illumination intensity (25 mW/cm^2) in this method the etching time which is divided into five steps ranging from 2-10 min and the current density is also varied into five from a higher value of about 25 mA/cm^2) to a lower value of about 5 mA/cm^2. Figure 2 shows the curve describes the gradient relation between current density with etching time. After that aluminum electrode was evaporated onto the surface of PSi and GPSi layer. Two sandwich structures of Al/PSi/n-Si/Al and Al/GPSi/n-Si/Al were fabricated to extract the electrical properties of porous silicon and the sensor's performance. The sensing process was carried out in a sealed cavity supplied with gas inlet and outlet at vacuum pressure with base pressure of about 10^{-5} Torr and with presence of CO_2 pressures of 0.5 and 1mbar at room temperature.

Preparation of PdNPs/PSi and PdNPs/GPSi structures: PSi and GPSi were modified with Pd NPs by an immersion plating process of as formed porous layer into $PdCl_2$ solution at room temperature. Both types of porous samples were inundated into the 5×10^{-2} M salt $PdCl_2$ solution for a fixed immersion time of 5 min to produce Pd NPs/PSi and PdNPs/GPSi structure. $PdCl_2$ solution was prepared by mixing (0.15 M HF with 5×10^{-2} M $PdCl_2$ and adding a few drops of HCl with concentration for about 37% at 60°C under magnetic stirring are about 60 min). The electro less deposition of Pd NPs through the dangling bonds of the porous layer occurs according to the following reactions, respectively (Alwan *et al*., 2015; Brahiti *et al*., 2015):

$$\begin{aligned} &Si+6HF \rightarrow H_2SiF_6+4H^+4e \\ &Pd^{2+}+2c \rightarrow Pd \end{aligned} \quad (1)$$

The schematic illustration of the processes for as formed PSi and GPSi and modified with Pd nanoparticles as shown in Fig. 3.

RESULTS AND DISCUSSION

Properties of PSi and GPSi layer: Porosity and the layer thickness of porous layer were determined by gravimetrical measurements (Ahmed *et al*., 2013). When comparing the porosity and layer thickness of the PSi and GPSi. We can see that the PSi has higher porosity and layer thickness than that of GPSi layer, this is because the gradual reduction of the photo-generation of carriers (e-h) in the deepest layer helps the pore growth and leading to an increase as layer thickness (Abdelrazek *et al*., 2014). Table 1 elucidates the porosity and layer thickness of PSi and GPSi layer.

FTIR spectra of PSi and GPSi layer: Chemical composition of porous layer was investigated by FTIR as shown in Fig. 3 and 4. From this figure, it's shown that the porous layer surface contains a high density of dangling bonds groups which include: wagging (Si-H), Si-H_2 and Si-H_3 (Bjorkqvist *et al*., 2004; Alwan and Abdulrazaq, 2008) and stretching modes of (Si-O-Si) due to the oxidation process of porous silicon at a specific wave number as illustrated in Table 2. The absorption peak of

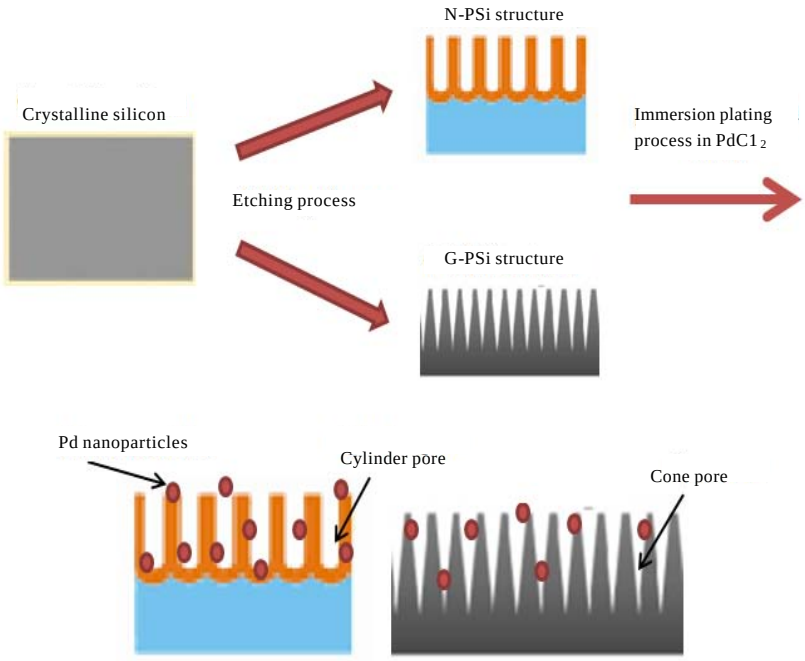

Fig. 3: Schematic illustration of the processes for PSi and GPSi modified with Pd nanoparticles

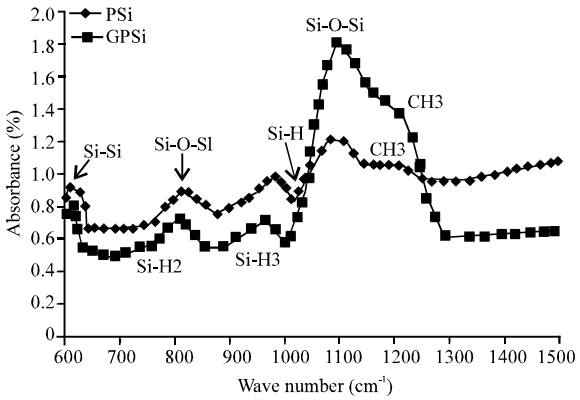

Fig. 4: FTIR spectra of as formed PSi and GPSi layer

Table 1: Porosity and layer thickness of PSi and GPSi

PSi	Porosity (%)	Layer thickness (μm)
PSi	67	36.145
GPSi	64	10.916

Table 2: Chemical composition of PSi and GPSi

Peak position (cm^{-1})	Attribution
621.24	Si-Si stretching
975	Si-H
858	Wagging Si-H2
945	Si-H3
1104, 815	Stretching modes (Si-O-Si)

GPSi is higher than that of PSi this is due to the large density of dangling bonds, so that, higher surface state (defects).

Morphological properties: The surface morphology of as-formed PSi and GPSi layer is present in Fig. 5. In the case of PSi, the surface consists of a pore-like structure with irregular shape (nearly circular form). The ranging of the pore is about 0.25-2.75 μm and the maximum size distribution is about 1.25 μm. For GPSi layer, the pore shape change from nearly circular pore form to star full form with gradient reduction in pores over sizes (gradient behavior) as a result of the dynamic etching including step reduction of etching current density (Alwan, 2014a, b). The dependence of pore diameter on the etching current density was studied by Huimin *et al.* (Ouyang *et al.*, 2005) and they reached, although, pore diameters were strongly dependent on the current density. As the current density decrease, the pore size decreases.

Figure 6 illustrates the morphological properties of Pd NPs/PSi and Pd NPs/GPSi structure. Figure 6 a-c shows the surface morphology of deposit Pd NPs on PSi and GPSi, respectively. As shown from the figure, palladium nanoparticles was aggregated mainly around pores walls, especially on PSi surface while for GPSi the Pd NPs was deposited in the outer shell of the pores and in the pores itself as shown in the cross section image. This behavior during the growth of metallic nanoparticles mainly related to the amounting and positions of dangling bonds groups (nucleation sites). For normal porous layer. Figure 7 shows the statistical distribution of Pd NPs on PSi and GPSi layers. The size distribution of Pd Nps is ranging 30-170 nm while for gradient porous layer, the

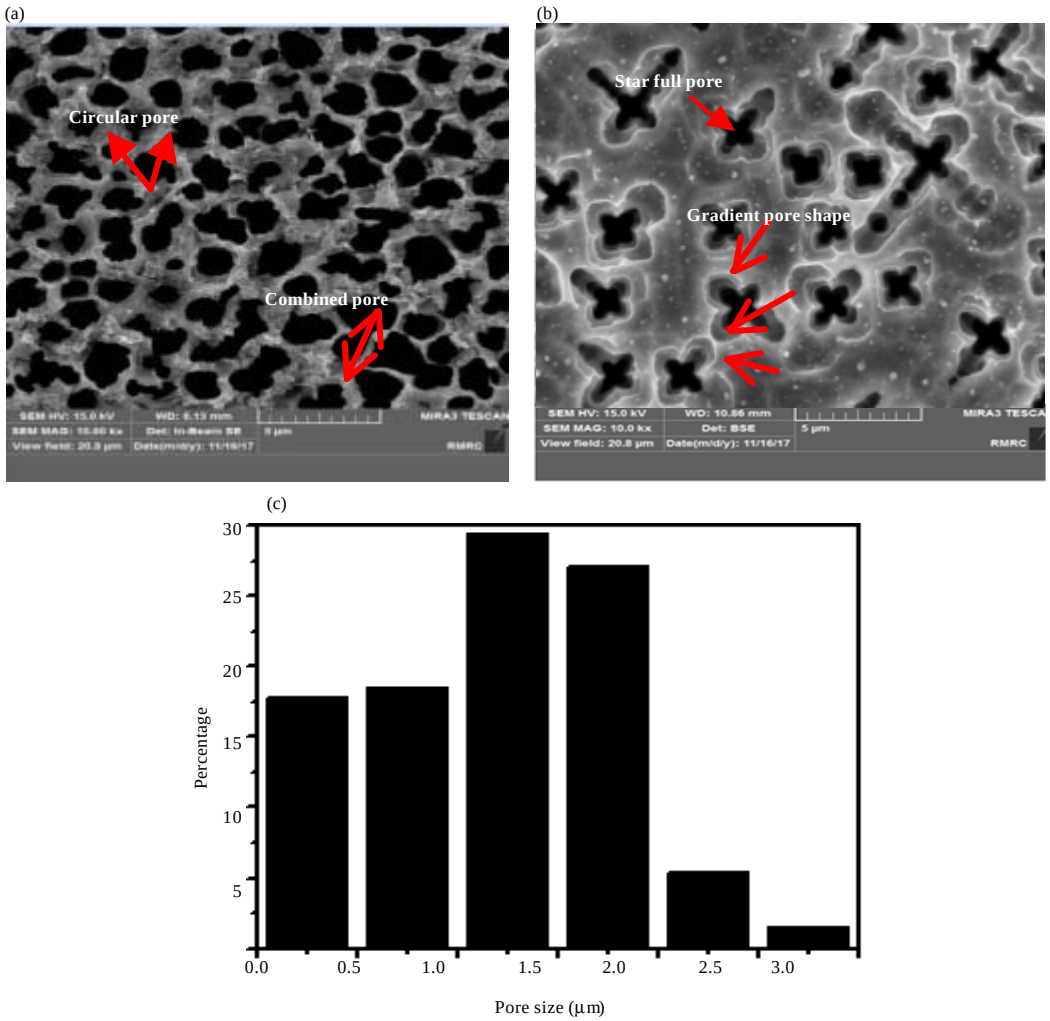

Fig. 5: SEM images of a) PSi layer; b) GPSi layer and c) Statistical pore size distribution

sizes of Pd NPs will range from 10-90 nm. These variations of Pd NPs sizes are related to the density of dangling bonds Si-Hx (x = 1-3) (nucleation sites) where the size's decrease with increasing nucleation sites. The surface of silicon regions is fully coated with dangling bonds (Si-H, Si-H2 and Si-H3) the types of nucleation sites are mainly depended on these bonds dihydrids Si-H2 and trihydrids Si-H3 these are widely located at the inner surface of the pores and the tips of silicon nano crystallites. Figure 6 c and d and Fig. 7 cross-section of N-PSi and G-PSi modified with nanoparticles.

XRD-characterization: XRD pattern is an effective device to determine the structure of NPs, Fig. 8, shows XRD for monometallic Pd NPs deposited on the PSi and GPSi planes at 40.4 and 46.8° these peaks which is conformity with reference data (JCPDS No. 271402) (Brahiti *et al*., 2015). The plane reflections (111) and (222) of Pd cubic (FCC) crystal. The crystalline size of NPs was calculated Sherre's equation (Jabbar *et al*., 2017). From these results, we found the particle size of Pd NPs/GPSi is smaller and have a higher specific surface area than particle size of Pd NPs/PSi, this is due to the gradient structure of the PSi have higher amounts of dangling bonds (nucleation sites). The Specific Surface Area (SSA) one of the facts of the worth of the nanostructured material it's given as (Jabbar *et al*., 2017):

$$SSA = \frac{6000}{D * \rho} \quad (3)$$

Where:

D = The particle size of Pd nanoparticles and

ρ = The density of palladium for about 12.023 (g/cm^3)

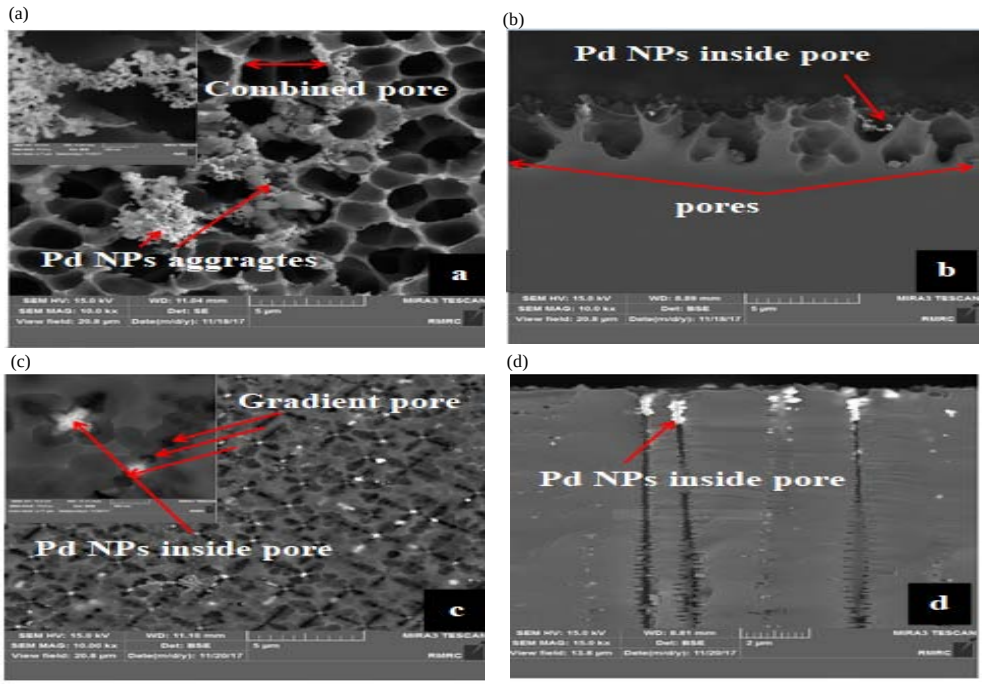

Fig. 6: SEM images of Pd NPs deposited on; a, c) PSi and GPSi and b, d) cross-section SEM images

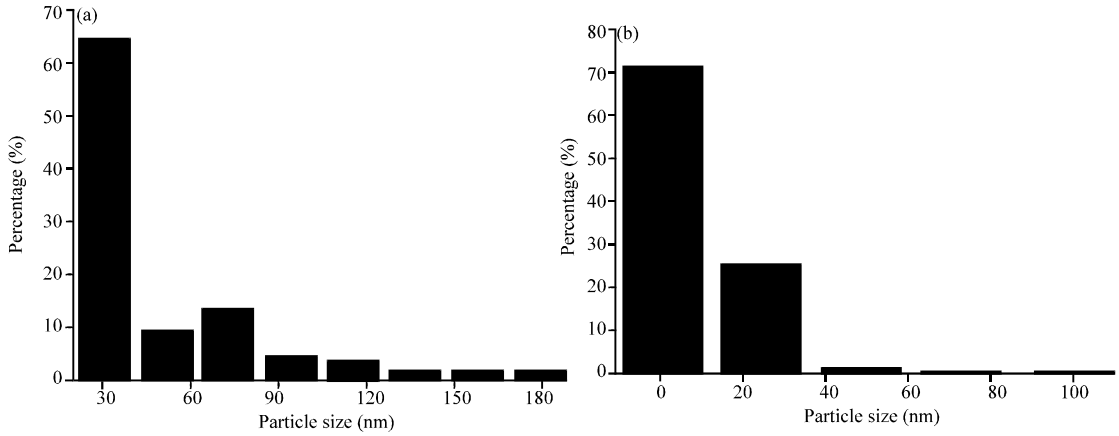

Fig. 7: Statistical distribution of Pd NPs sizes on; a) PSi and b) GPSi

Table 3: Particle size and Specific Surface Area (SSA) of Pd NPs

	Phase (111)		Phase (200)	
Hetro structure	Nanoparticles	SSA (m^2/g)	Nanoparticles size (nm)	SSA (m^2/g)
Pd NPs/PSi	30.0	16.55	24.13	20.68
Pd NPs/GPSi	15.4	32.40	10.00	49.90

Table 3, demonstrates the grain size and Specific Surface Area (SSA) of the Pd NPs/PSi and Pd NPs/GPSi in the phase (111) and (200) on PSi layer.

EDS analysis: Energy-dispersive X-ray spectroscopy EDS was used to provide nanoparticles percentages in the porous structure. Figure 9a and b shows that the intensity of Pd NPs peak in the GPSi is higher than that the intensity of Pd NPs peaks in the PSi the percentages of the Pd NPS on the gradient layer is higher than that of normal layer, this is due that GPSi has large amounts of dangling bond groups. From this composition, analysis confirms the growth of NPs and the presence of Si and O elements and no other elements were found.

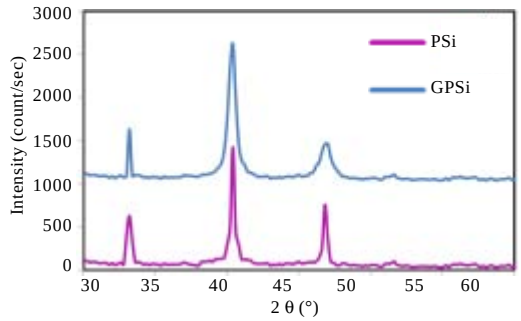

Fig. 8: XRD pattern of Pd NPs/PSi and Pd NPs/GPSi

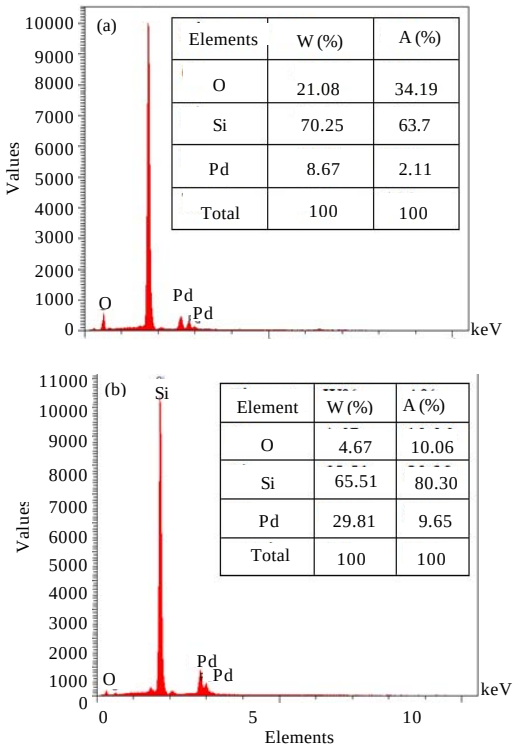

Fig. 9: EDS analysis of a) Pd/N Pd NPs/PSi and b) Pd Nps/GPSi structure

Electrical properties of Al/PSi/n-Si/Al and Al/ GPSi/n-Si/Al structure: Electrical properties of Al/PSi/n-Si/Al and Al/GPSi/n-Si/Al sandwich structures were fabricated to calculate the electrical properties of porous silicon in dark conditions at room temperature with voltage ranging from (0-5V) is shown in Fig. 10. We found the forward current in the PSi is higher than that of GPSi this is as a result of GPSi has a large density of dangling bonds on the porous surface (Hwang *et al*., 2011). The rectifying behaviors were recorded in for PSi sample while for GPSi sample a semi-linear relationship was observed due to the existing of surface state (Sze, 1985). Based on the existence of Schottky is like junction. Charge carrier transport mechanism across the barrier is governed by thermionic emission; J_0 is given by the expression (Alwan and Jabbar, 2011):

$$J_0 = A^*T^2 \exp\left[\frac{-\phi_{Bn}}{KT}\right] \quad (4)$$

where, A* is the effective Richardson which equal to 120 ($A/K^2.cm^2$) for n-type silicon from the Eq. 5 the barrier height is given by Sze (1985):

$$\phi_{Bn} = \frac{K_B T}{q} \ln\left(\frac{A^{**}T^2}{I_s}\right) \quad (5)$$

The important electrical characteristic for a Schottky like junction (PSi) can be calculated ideality factors n was calculated according to the following Eq. 6 (Sze, 1985):

$$n = \frac{q}{K_B T} \frac{\Delta V}{\ln \frac{I}{I_s}} \quad (6)$$

The high value of the ideality factor in porous silicon layer is due to the presence of high amounts of the interface states at the porous silicon boundaries is given by the following Eq. 7 (Sze, 1985):

$$n = 1 + \frac{\delta_{\epsilon_s}}{w\epsilon_i} + \frac{\delta_q D_s}{\epsilon_i} \quad (7)$$

Where:

D_s = The state density (cm^{-2} eV^{-1}) dangling bonds groups presented in the interface layer of the porous structures

W = The thickness of the PSi layer

ϵ_i, ϵ_s = The dielectric constant for the porous silicon and semiconductor regions (silicon), respectively

The value of (ε_i) is a function to the porosity of the porous layer can be calculated by using (Wail *et al*., 2015) with (ε_{si}) = (11.9) and (ε) is the thickness of the interface layer is about 25 nm (Peng *et al*., 1996). Table 4 show the electrical parameters of the formed junction (saturation current, barrier height, ideality factor and D_s state density (dangling bonds). From this table, we noticed the barrier height ideality factor and dangling bonds for GPSi are larger than that of PSi.

Electrical properties of Al/Pd NPs/ PSi/Si/Al and Al/ Pd NPs/GPSi/Si/Al hetro structure: J-V characteristics of

Table 4: Electrical parameters of PSi and GPSi structure

Hetro structure saturation	Current (μA)	Barrier height Φ_{Bn} (eV)	Ideality factor (n)	D_s state density (Dangling bond) 1/cm^2 eV
PSi	100	0.596	7.7	0.757×10^{19}
GPSi	800	0.721	23.2	2.67×10^{19}

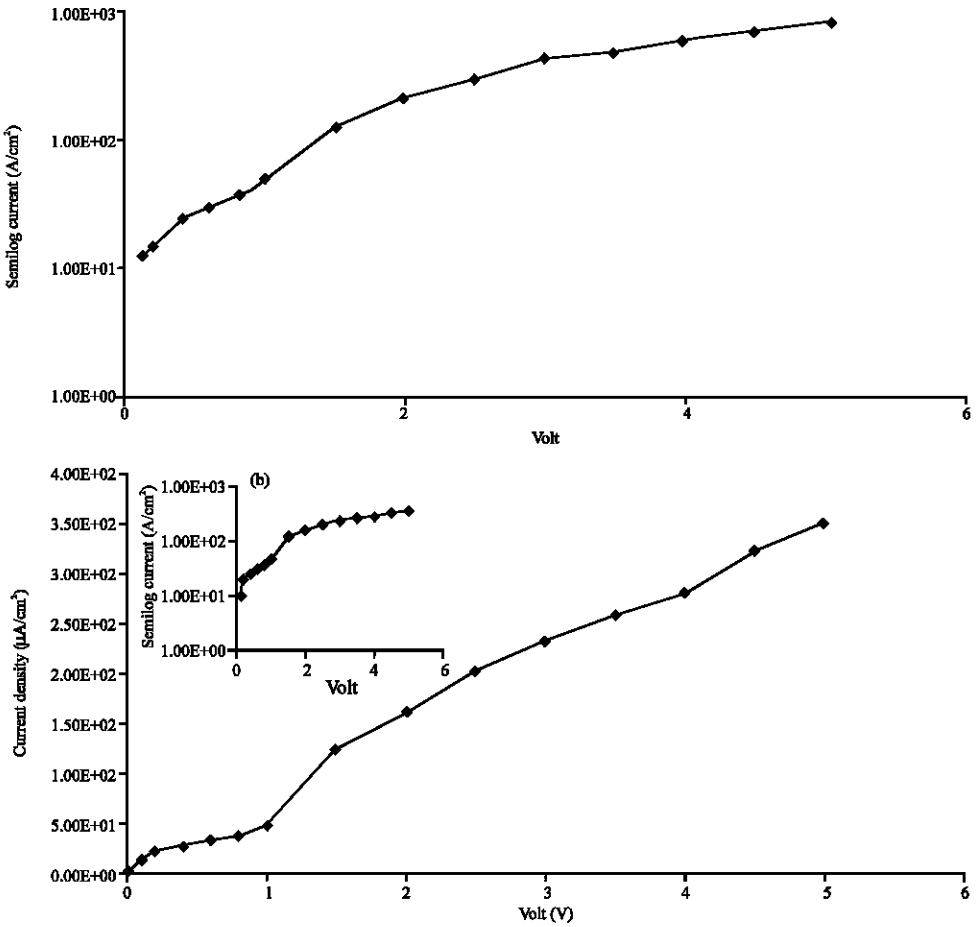

Fig. 10: J-V characteristics of a) Al/ PSi/n-Si/Al and b) Al/ GPSi/n-Si/Al, inset these figure curves of semi log of current

the Pd NPs modified PSi and GPSi gas sensor at two gas pressures 1 and 0.5 mbar are done at room temperature in dark conditions with voltage ranging from (0-5 V) as shown in Fig. 11. For both types of sensor hetro structure, the J-V characteristics show a rectifying behavior due to exist of Schottky like junction between the Pd NPs and porous silicon layer (Razi *et al*., 2010). In the presence of CO_2 gas molecule, the forward current of the GPSi hetro structure is higher than that of PSi. This is due to GPSi has a higher sensitivity to the CO_2 gases than PSi because high nucleation sites in GPSi lead to more gas molecule adsorption inside pores (pores have different shape) (Hwang *et al*., 2011; Alwan, 2014a, b). The relative response of the current sensitivity of the hetro structure sensor was calculated using the following relation (Alwan *et al*., 2017):

$$\text{Senstivity} = \frac{\text{Igas-Iw}}{\text{Iw}} \quad (8)$$

where, Igas and Iw represent the current in the presence and absence of CO_2 gas, respectively. Figure 12a and b, shows the sensitivity-voltage characteristics of Al/Pd NPs/PSi/n-Si/Al and Al/Pd NPs/GPSi/n-Si/Al hetrostructures under two concentrations of CO_2 (0.5 and 1 mbar) gas at room temperature. The maximum response was obtained for a GPSi layer compared with PSi layer, the maximum sensitivity of about 5.4% is observed at a bias voltage of about 1.5 V for GPSi compared to the about 3% at bias voltage 0.2 and 1.8 for PSi, respectively. This is attributed to the existence of Schottky barrier the current is strong well-ordered by the change in Φ_{Bn} which is formed between the Pd

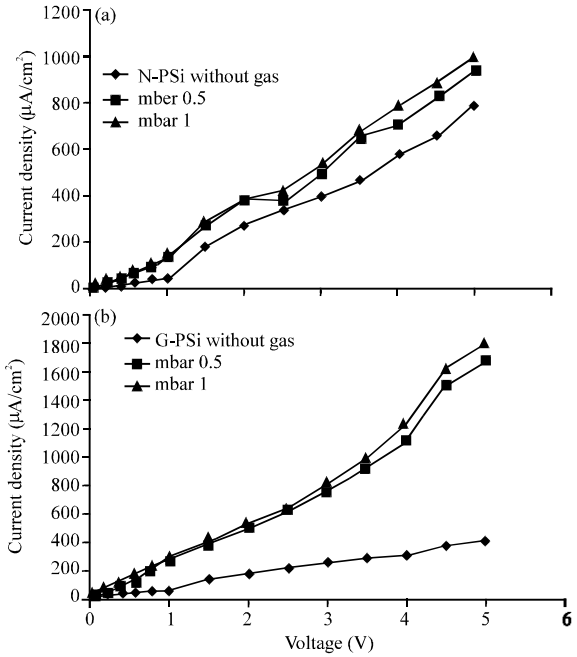

Fig. 11: J-V characteristics of a) Al/PdNPs/ PSi/Si/Al and b) Al/PdNPs/GPSi/Si/Al hetro structure after exposure to CO_2 gases

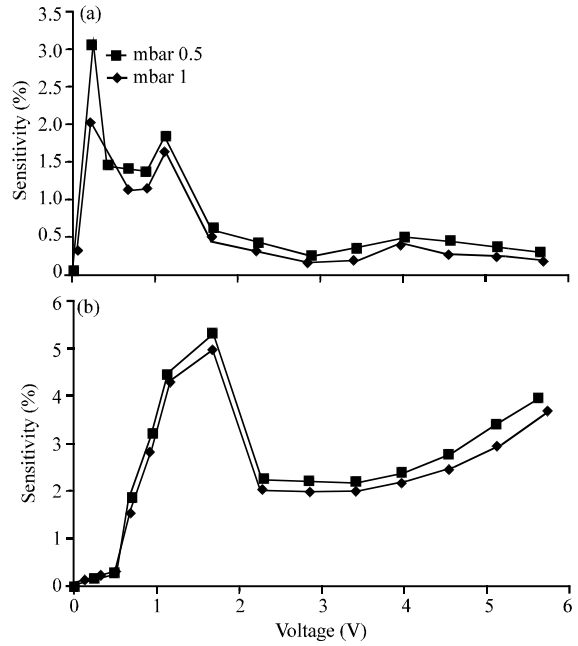

Fig. 12: Sensitivity vs. voltage of a) Al/Pd NPs/ PSi/Si/Al and b) Al/Pd NPs/GPSi/Si/Al hetro structure at room temperature

NPs layer and porous layer in addition to the specific surface area and the density of Pd NPs nanoparticles.

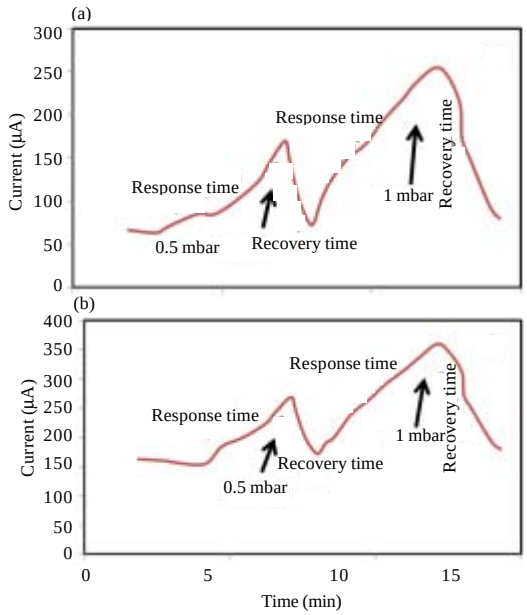

Fig. 13: Response and recovery time of a) Al/PdNPs/ PSi/Si/Al and b) Al/PdNPs/GPSi/Si/Al hetro structure at room temperature

Table 5: Temporal response of (a) Al/Pd NPs/PSi/Si/Al and (b) Al/Pd NPs/GPSi/Si/Al hetro structure at room temperature

	Hetro structures		CO_2 concentrations	
	Response time (min)		Recovery time (min)	
Variables	0.5 (mbar)	1 (mbar)	0.5 (mbar)	1 (mbar)
Pd NPs/PSi	4.10	4.70	2.70	5.00
Pd NPs/GPSi	0.69	0.72	0.25	0.43

Response time and recovery time characteristics of the Al/Pd NPs/PSi/n-Si/Al and Al/Pd NPs/GPSi/n-Si/Al hetro structures with two gas pressures at room temperature is presented in Fig. 13 at the optimum biasing applied Voltage 2V. Table 5 shows the results of response and the recovery time, these results showed that the sensor with GPSi has significant short response and recovery times compared with a PSi layer because of the high rate of CO_2 gas adsorption in the GPSi structure due to the high density of dangling bonds.

CONCLUSION

In this comparative study, hetro structures CO_2 gas sensors were fabricated by modifying normal and gradient PSi layer with Pd nanoparticles. It has been observed that the sensor performance depends greatly on the nanoparticle types, size's distribution and on pore morphology. Highest sensitivities with minimum response and recovery times were succeeded in the GPSi layer compared with PSi layer. The enhanced performance of

sensors was attributed to the high integrated specific surface area of the nanoparticles and the role of the dangling bonds in the interface inside the silicon matrix to increase adsorption of gas molecules inside pores. Finally, from this study, we obtained a sensitive gradient porosity porous silicon gas sensor with fast response time and recovery time as a result of pore morphology and dangling bonds of porous matrix.

ACKNOWLEDGEMENTS

The researchers would like to acknowledge the Department of Applied Sciences-University of Technology, Nanotechnology and Advanced Materials Research Center-University of Technology and Razi Metallurgical Research Center-Iran for their facility and assistance to use the SEM (MIRA3 TESCAN) device and conducting the EDS analyses. The financial support is also acknowledged.

REFERENCES

Abdelrazek, E.M., A.M. Alwan, M. Kamal and W.H. Ali, 2014. Spectroscopic aspects of gradient-porosity system. Intl. J. Eng. Sci. Res. Technol., 3: 298-306.

Ahmed, L.B., S. Naama, A. Keffous, A. Hassein-Bey and T. Hadjersi, 2015. H2 sensing properties of modified silicon nanowires. Prog. Nat. Sci. Mater. Intl., 25: 101-110.

Ahmed, N.M., Y. Al-Douri, A.M. Alwan, A.A. Jabbar and G.E. Arif, 2013. Characteristics of nanostructure silicon photodiode using laser assisted etching. Procedia Eng., 53: 393-399.

Alwan, A.M. and A.A. Jabbar, 2011a. Design and fabrication of nanostructures silicon photodiode. Mod. Appl. Sci., 5: 106-112.

Alwan, A.M. and A.B. Dheyab, 2017b. Room temperature CO2 gas sensors of AuNPs/mesoPSi hybrid structures. Appl. Nanosci., 7: 335-341.

Alwan, A.M. and O.A. Abdulrazaq, 2008. Aging effect on the photosynthesized porous silicon. Intl. J. Mod. Phys. B, 22: 417-422.

Alwan, A.M., 2014. An investigation of multi-porous silicon gas sensor. Eng. Technol. J., 32: 183-190.

Alwan, A.M., 2014. The Opto-electronic characteristics of multi-porosity silicon system. Eng. Technol. J., 32: 191-197.

Alwan, A.M., A.A. Yousif and L.A. Wali, 2017. The growth of the silver nanoparticles on the mesoporous silicon and macroporous silicon: A comparative study. Indian J. Pure Appl. Phys., 55: 813-820.

Alwan, A.M., A.J. Hayder and A.A. Jabbar, 2015. Study on morphological and structural properties of silver plating on laser etched silicon. Surf. Coat. Technol., 283: 22-28.

Alwan, A.M., R.A. Abbas and A.B. Dheyab, 2018. Study the characteristic of planer and sandwich PSI gas sensor (comparative study). Silicon, 1: 1-8.

Bjorkqvist, M., J. Salonen, J. Paski and E. Laine, 2004. Characterization of thermally carbonized porous silicon humidity sensor. Sens. Actuators A Phys., 112: 244-247.

Brahiti, N., T. Hadjersi, H. Menari, S. Amirouche and O.E. Kechai, 2015. Enhanced photocatalytic degradation of methylene blue by metal-modified silicon nanowires. Mater. Res. Bull., 62: 30-36.

Fabricius, H., 1992. Gradient-index filters: Designing filters with steep skirts, high reflection and quintic matching layers. Appl. Opt., 31: 5191-5196.

Hwang, J.D., S.B. Hwang, C.H. Chou and Y.H. Chen, 2011. Investigation of opto-electronic properties on gradient-porosity porous silicon layer. Thin Solid Films, 519: 2313-2316.

Jabbar, A.A., A.M. Alwan and A.J. Haider, 2017. Modifying and fine controlling of silver nanoparticle nucleation sites and SERS performance by double silicon etching process. Plasmonics, 13: 1171-1182.

Ogata, Y.H., A. Koyama, F.A. Harraz, M.S. Salem and T. Sakka, 2007. Electrochemical formation of porous silicon with medium-sized pores. Electrochem., 75: 270-272.

Ouyang, H., M. Christophersen and P.M. Fauchet, 2005. Enhanced control of porous silicon morphology from macropore to mesopore formation. Phys. Status Solidi A, 202: 1396-1401.

Peng, C., K.D. Hirschman and P.M. Fauchet, 1996. Carrier transport in porous silicon light-emitting devices. J. Appl. Phys., 80: 295-300.

Razi, F., A.I. zad and F. Rahimi, 2010. Investigation of hydrogen sensing properties and aging effects of schottky like Pd/porous Si. Sensors Actuators B: Chem., 146: 53-60.

Starkov, V. and E. Gavrilin, 2007. Gradient-porous structure of silicon. Phys. Stat. Sol., 4: 2026-2028.

Striemer, C.C. and P.M. Fauchet, 2002. Dynamic etching of silicon for broadband antireflection applications. Appl. Phys. Lett., 81: 2980-2982.

Sze, S.M., 1985. Semiconductor Devices-Physics and Technology. John Wiley & Sons, Hoboken, New Jersey, USA., Pages: 523.

Wail, H.A., M.K.M.Y.K. Kamal, A.M. Alwan and E.M. Abdelrazek, 2015. Synthesis and characterization of nanostructured silicon as anti-reflection layers for optoelectronic applications. J. Mater. Sci. Photon, 121: 214-220.